ORIGINAL PAPER

Luminescence Enhancement from Silica-Coated Gold Nanoparticle Agglomerates Following Multi-photon Excitation

Sviatlana Viarbitskaya · Linus Ryderfors ·
Therese Mikaelsson · Emad Mukhtar ·
Lennart B.-Å. Johansson

Abstract Multi-photon absorption induced luminescence (MAIL) from bare gold nanoparticles, silica-coated particles, as well as silica-coated agglomerated gold nanoparticles suspended in aqueous solution was studied by using time-resolved and steady-state luminescence spectroscopy. The nanoparticles were excited by femtosecond pulses of wavelengths ranging from 630 nm to 900 nm. The luminescence from the particles exhibits a broad spectrum in the UV and VIS region. The time-resolved measurements indicate a luminescence lifetime of a few ps, limited by the response of the experimental system. The studied dependence of the MAIL efficiency on the excitation wavelength showed that the luminescence from silica-coated agglomerates was enhanced over the whole range of excitation wavelengths, when compared to the luminescence from individual gold nanoparticles. The agglomerates show an almost excitation wavelength independent efficiency of the MAIL, while for individual nanoparticles a rapid decrease of the MAIL efficiency was observed with increasing excitation wavelength. The observed enhancement of the MAIL from the agglomerated nanostructures can be attributed to the presence of localized surface plasmon resonances in the spectral region corresponding to the excitation wavelengths. The high MAIL efficiency from the agglomerated nanoparticle structures in the near-infrared could be an advantage in the expanding field of luminescence-based-imaging, as well as in biosensor technology.

Keywords Surface plasmon · Time-resolved ps detection · Extinction spectra · UV-VIS-NIR

Abbreviations

AuNPs	gold nanoparticles
LSPR	localized surface-plasmon resonance
NP	nanoparticle
SERS	surface enhanced Raman scattering
TEM	transmission electron microscopy
TCSPC	time-correlated single photon counting
MAIL	multi-photon absorption induced luminescence
OD	optical density

S. Viarbitskaya · L. Ryderfors · E. Mukhtar
Department of Photochemistry and Molecular Science,
Uppsala University,
P.O. Box 523, 751 20 Uppsala, Sweden

E. Mukhtar
e-mail: emad.mukhtar@fotomol.uu.se

T. Mikaelsson · L. B.-Å. Johansson (✉)
Department of Chemistry, Umeå University,
901 87 Umeå, Sweden
e-mail: lennart.johansson@chem.umu.se

Introduction

The spectacular optical properties of nanoparticles (NPs) formed from noble metals have long been a subject of theoretical and experimental interest [1–4]. The optical properties of these NPs are ascribed to localized surface-plasmon resonance (LSPR). The LSPR arises from collective oscillations of the surface charge density, which are induced by incident electromagnetic radiation. The position and width of the LSPR depend on the particular material, its size, shape, as well as its interactions with the environment and the proximity of other NPs [5–8]. The excitation of a LSPR leads to the confinement of electromagnetic energy in regions at the particle surface, whereby strong and localized electromagnetic fields are created. One interesting property of these localized electromagnetic fields is their

ability to enhance radiative rates in various linear and nonlinear optical processes at metal surfaces. This phenomenon has been utilized for the development of various "surface-enhanced" techniques, such as surface-enhanced Raman scattering (SERS) [9, 10], surface-enhanced one- and multi-photon fluorescence [11, 12] and surface-enhanced second-harmonic generation (SESHG) [9, 10, 13]. Gold and other metal NPs have been used in different technological, biological and medical applications. For instance, in solar energy conversion, reaction catalyses, biosensors, imaging microscopy and in medical diagnostics [9, 10].

Multi-photon absorption induced luminescence (MAIL) from noble metals was first observed in 1981 by Chen et al [13]. The luminescence was attributed to a radiative recombination of the electrons excited from the d bands to the s-p conduction levels above the Fermi level [14–16]. Other mechanisms have been suggested, such as radiating plasmons of NPs [17, 18] and a localized IR surface plasmon enhanced s-p intraband radiative transition [19]. It has also been discussed whether the observed luminescence is due to an interplay between these processes [20]. At present, however, the mechanism of luminescence from metal NPs is still a question under debate.

It has been observed that the MAIL from roughened surfaces is several orders of magnitudes stronger than that from flat surfaces. This is ascribed to a local-field enhancement caused by nano-sized curvatures at the metal surface [13, 14]. It has also been suggested that the main contribution to the observed nonlinear luminescence spectra emanates from surface atoms localised where the local fields are strongest [14]. This implies that the MAIL is much more sensitive to properties of the LSPR than its linear analogue. This theoretical model of local-field enhancement, was applied successfully for explaining the observed luminescence enhancement from silver nanoparticles of different size, excited at different wavelengths [21]. The enhanced MAIL was also observed from AuNPs embedded in SiO_2 films, single AuNP aggregates on glass surfaces, as well as from AuNPs in solutions [17, 18, 22, 23].

Strong luminescent enhancement has been observed from aggregated and agglomerated noble metal NPs [6–8, 24–26]. In agglomerates, the near-field interaction between NPs leads to strong local electric fields in the vicinity of particle surface, so called "hot spots" [22]. These cause several multi-polar surface plasmon resonances, which are red-shifted as compared to the individual NP spectrum [6, 8, 21, 24, 26]. The near-field interaction is extremely sensitive to the interparticle distance, as well as the particle size and shape. One can therefore manipulate these parameters in order to maximize the luminescence enhancement. A notable example is the plasmonic interactions within a dimer of NPs, which is the simplest agglomerate system [6, 8, 17]. It was shown theoretically and experimentally that LSPR energies can change considerably with interparticle distances and particle sizes [6, 8, 24–26].

This article reports on the first observation of a MAIL enhancement from agglomerates of AuNPs by two orders of magnitude, as compared to the luminescence from individually suspended spherical nanoparticles in solution. The enhancement is reported as a function of excitation wavelength in the interval of 630–900 nm. Our observations support the theory, which states that the electromagnetic field enhancement is due to the coupling between the incident radiation and the LSPR of NP agglomerates.

Experimental Section

Sample Preparations

Chemicals

NH_4OH (25% aqueous solution) from Scharlau, 2-propanol and N-cetyl-N, N, N-trimethylammoniumbromide (CTAB) from Merck, tetraethylorthosilicate (TEOS, 99.999%) and sodium borohydride (99,9%) from Sigma-Aldrich, trisodium citrate dihydrate (Na-cit, ≥99,5%) from Riedel-de Haën, $HAuCl_4$.aq (≥49% Au) from Fluka. All chemicals were used as received. The water used for all preparations were run through Milli-Q water purification system with a resistivity of at least 18 MΩ·cm.

Preparation of Gold Nanoparticles

In the preparation of pure gold nanoparticles, gold salt was reduced by sodium citrate, as previously described [27], but with the difference that the surfactant CTAB and the base NaOH was present during the preparation. Shortly, 18 mL of a 0.1 M CTAB solution was mixed with 0.5 mL 0,01 M $HAuCl_4 \cdot H_2O$, 0.5 mL of 0.01 M trisodium citrate and 0.5 mL 0.1 M NaOH, all aqueous solutions. To this, 0.5 mL of freshly prepared 0.1 M $NaBH_4$ solution was added all at once and mixed before left undisturbed for some time. The solution was kept in a water bath maintained at 25°C. This preparation resulted in gold nanoparticles with a diameter of 4–6 nm.

The gold nanoparticles used for silica coating was prepared by another method [28]. Shortly, 200 mL of 0.24 mM $HAuCl_4$ in H_2O was heated to 80°C before 0.94 mL of 0.34 M Na-Cit in H_2O was added under vigorous stirring. The colour turned wine red within 15 min and the solution was left to cool after 30 min. This method yields gold nanoparticles of average diameter 15 nm.

Preparation of Silica Coated Gold Nanoparticles

The silica coating of the gold nanoparticles was performed as previously described by E. Mine et al. However, 2-propanol was used instead of ethanol. The synthesis was performed using a method where a mixture of water/gold particles/2-propanol was stirred vigorously before the addition of first TEOS and second aqueous ammonia, which initiated the silica coating. The samples were left with stirring for 24 h in room temperature. The suspensions were then washed and centrifuged three times with 2-propanol and water, respectively, before re-suspended in water. Centrifugation was performed at 20°C, 10 000 rpm and 10 min. The thickness of the silica layer was controlled by varying the amount of TEOS.

Sample Characterisation

Properties of the four samples (**I–IV**) studied are given in Table 1. The transmission electron microscopy (TEM) images of the NPs are shown in Fig. 1. Samples **I** and **II** consist of spherical naked AuNPs (diameter 5±1 nm) and SiO_2 coated AuNPs (diameter 12±4 nm), respectively. The TEM image of **II** reveals the presence of a small number of dimers (*cf.* Fig. 1b). However the concentration of dimers is negligible in comparison to the abundance of individually SiO_2coated NPs. Samples **III** and **IV** contain suspended SiO_2-coated agglomerates of AuNPs with the mean core diameter of 12±2 nm and a coating thickness of 170± 20 nm and 300±35 nm, respectively. The average number of AuNPs in a silica particle core is about two times higher in sample **IV**, as compared with sample **III**. It can be assumed that the studied agglomerates are intrinsically 3D structures, although this cannot be observed from an inspection of the 2D TEM images.

Due to the sample heterogeneity, it was difficult to determine the exact AuNP concentrations. In order to avoid concentration dependence effects, the samples were diluted to the same maximum OD(520 nm)=0.1 in 1.0 cm cuvettes.

Table 1 The shorthand notation and description of the AuNP samples studied in this work

| Code	Sample description
I	Single spherical AuNPs with the diameter of 4–6nm
II	Silica coated single spherical AuNPs with the core diameter of 8–16nm and silica shall thickness of 30–75nm.
III	Silica coated agglomerated AuNPs. Diameter of a single AuNPs is 10–14nm. Silica shall thickness is 150–190nm. Each particle contains up to 10AuNPs in the core.
IV	Silica coated agglomerated AuNPs. Diameter of a single AuNPs is 10–13nm. Silica shall thickness is 265–335nm. Each particle contains up to 20AuNPs in the core.
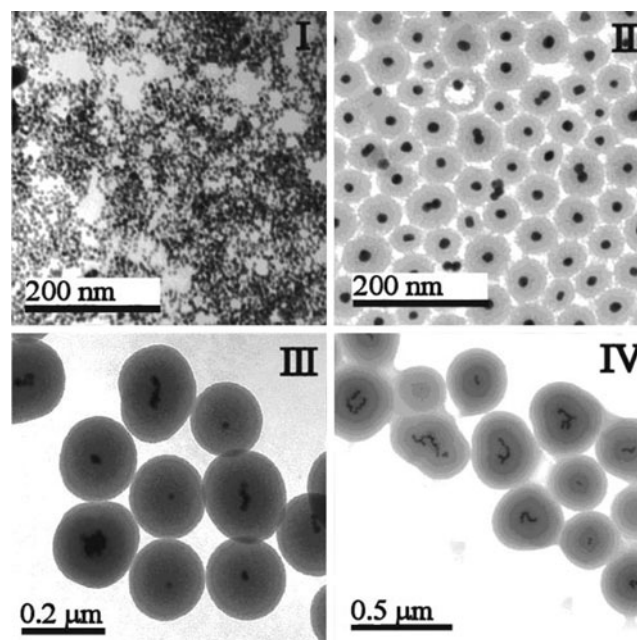
Fig. 1 TEM images of the studied samples **I** (**a**), **II** (**b**) **III** (**c**) and **IV** (**d**). The characteristic properties of the samples are summarised in Table 1

The detected MAIL intensity from all samples depends linearly on the particle concentration.

TEM

Formvar-coated 200 mesh Cu/Ni grids were placed on Parafilm and 20 uL of the sample was put on top of the grids for 30 min to sediment particles by gravity to the film. The grids were then removed, excess sample was dried by pointing the edge of the grid to a filter paper and final drying was done for at least 6 h in room temperature before microscopy. All samples were analyzed in a JEOL JEM 1230 transmission electron microscope and appearances of the samples were assessed with magnifications between 80.000× and 150.000×. Measurements of particle sizes were performed both directly in the microscope and from saved images.

Apart from the four samples discussed in this article, other samples were examined during the course of experiments. Those samples were composed of naked and silica coated individual spherical AuNPs. The MAIL properties of these samples were similar to those discussed in this article (*cf.* Table 1). For clarity reasons, the results obtained from these samples have not been reported here.

In order to estimate the strength of the MAIL from AuNPs, one can compare with a standard two-photon reference. Here a 1 μM methanol solution of Rhodamine 6G was used, which has a two-photon absorption cross-section of 65 Göppert-Mayer [29]. In the present study of

samples **III** and **IV** (λ_{exc}=800 nm) the MAIL intensity was weaker by two orders of magnitude.

Experimental System

The laser source was a 1 kHz Ti:Sapphire amplifier (Legend, Coherent) pumped by a frequency doubled Q-switched Nd:YLF laser (Evolution-30, Coherent) and seeded by a mode-locked Ti: Sapphire oscillator (Vitesse-800, Coherent). The output at 800 nm was directed to an optical parametric amplifier (TOPAS, Light Conversion). The excitation wavelengths between 630 and 900 nm were obtained by frequency doubling of the TOPAS signal which was tuneable in the range of 1260–1800 nm. The excitation beam was linearly polarised; the pulse duration and the spectral width were dependent on the wavelength, and was measured to be in the range of 160–210 fs, and 9–15 nm, respectively. Care was taken to eliminate the IR idler and signal beams generated by the TOPAS and propagating along the excitation beam. Colour glass filters were used to block the IR and VIS super-fluorescence of the TOPAS output.

The excitation beam was focused into the sample, which was contained in standard fused silica cuvette. The emission from the samples was collected at right angle to the excitation beam by a bi-convex lens and using a monochromator (ARC SpectraPro-150, 1800 g/mm density and blaze wavelength of 500 nm) equipped with a photo-multiplier tube detector (R928, Hamamatsu). A BG42 glass filter was used to suppress scattered laser light. In order to improve the signal-to-noise ratio the PMT output was analyzed by means of gated integrator and boxcar averager (Stanford Research System). White light generation from a particle suspension could be observed when the pulse energy was about 200 nJ and higher. Hence all the measurements reported here were performed at excitation energies lower than 200 nJ/pulse.

The time-resolved measurements of the MAIL were carried out by means of a streak camera detection (C5680, Hamamatsu). The excitation source was a 200 kHz amplified Ti:Sapphire operating at 800 nm with pulses width of 120 fs [30]. Extinction spectra were recorded on a UV-VIS-NIR spectrophotometer (Cary 5000, Varian).

Results

Extinction Spectra

The extinction spectra of samples **I–IV** are displayed in Fig. 2. Sample **I** shows a distinct surface plasmon extinction band, with a peak maximum at approximately 523 nm. The rising part of the spectra at shorter wave-
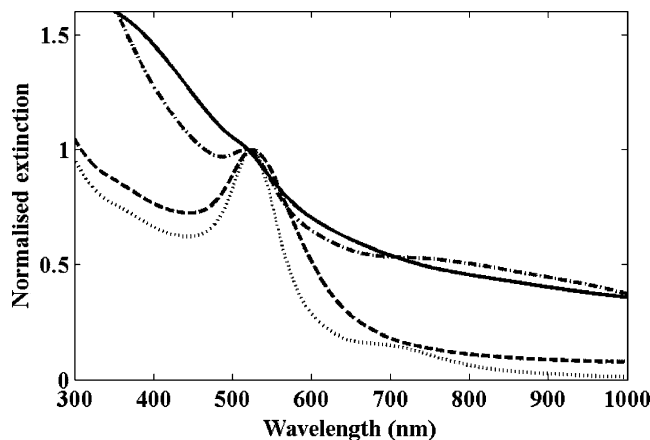

Fig. 2 Extinction spectra of the studied samples: **I** (dashed curve), **II** (dotted curve), **III** (dash-dotted curve) and **IV** (solid curve). All the curves were normalised to unity at the maximaum of the corresponding LSPR peak centred at approximately 520 nm

lengths is due to the onset of interband transitions between the 5d and 6s-p bands near the L point of the band structure [18]. Sample **II** exhibits a similar extinction spectrum as sample **I**, but also a weaker band centred at approximately 700 nm, which can be attributed to the presence of a small amount of agglomerated AuNPs in the core (cf. Fig. 1b). The broadening of the plasmon absorption band linewidth in sample **I** in comparison to **II** is likely a manifestation of plasmon oscillation damping due to scattering of electrons at the NP interface [31].

The extinction spectra of samples **III** and **IV** are dominated by Rayleigh scattering. For sample **III**, two LSPR bands are observed, with peak maxima centred at approximately 520 and 800 nm. These bands can be explained by an agglomeration, as was also detected in sample **II**. The thicker SiO$_2$-coating (300±35 nm) in Sample **IV** causes a stronger Rayleigh scattering, which makes it difficult to localise the positions of the LSPR peaks. This and the large diversity of the agglomerated structure in sample **IV** could account for the lack of additional features in its spectrum.

Photoluminescence Properties

Typical MAIL emission spectra from the samples are displayed in Fig. 3. These spectra were not corrected for the wavelength dependent sensitivity of the detectors. The spectra were broad with a peak maximum centred approximately at 440 nm. None of the samples exhibited any signal arising from hyper-Rayleigh scattering, or second-harmonic generation. This suggests that contributions from these second-order nonlinear processes are much weaker than the MAIL. A shoulder observed at ca. 600 nm was caused by Rayleigh scattering of the excitation light and transmission properties of the BG42 glass filter. No
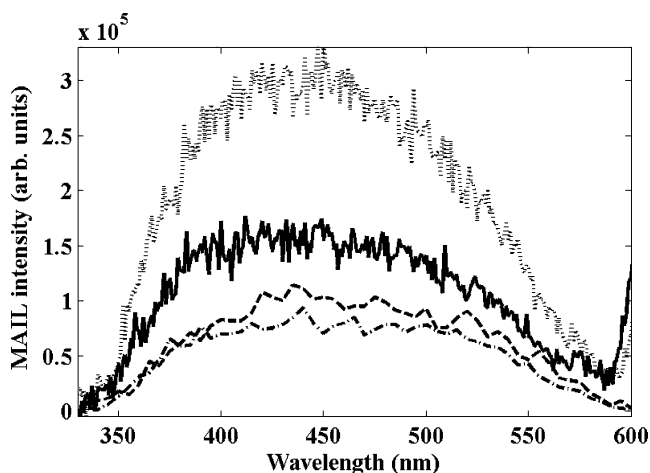
Fig. 3 MAIL emission spectra obtained for sample **I** (dashed curve), **II** (dash-dotted curve), **III** (dotted curve) and **IV** (solid curve) and the excitation wavelength 630 nm

significant change in the shape of MAIL spectra obtained from different NPs was observed. Neither the excitation power nor the excitation wavelength did significantly influence the MAIL spectra. Previously an emission spectrum identical to those shown in Fig. 3 was reported by Zhu et al [16]. In their study AuNPs were excited with the 1064 nm laser beam, and the observed emission was attributed to three-photon absorption induced process.

The dependence of the integrated MAIL intensity (I_{MAIL}) on the averaged excitation power (W_A) suggests a quadratic dependence for low excitation power in the wavelength region 450–530 nm. At higher excitation power, the slope level off, as shown in Fig. 4. A similar behaviour was reported on similar systems by others [16].
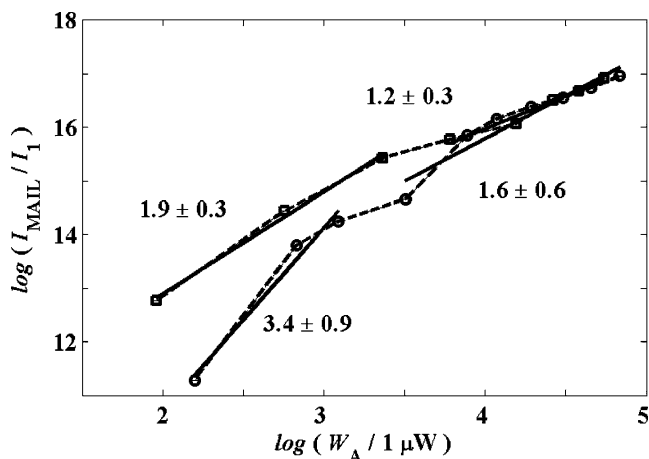

Fig. 4 Dependence of the integrated MAIL intensity, I_{MAIL}, on the averaged incident power, W_A. The data correspond to the excitation wavelength 850 nm and for sample **III**. Data points denoted with squares correspond to the intensity I_{MAIL}, calculated for the wavelength range 450–590 nm, while data points with circles refer integrated intensities for the range 290–390 nm. I_1 is the reference intensity. Next to each straight line, its slope is given

Power dependent measurements at shorter wavelengths (290–390 nm) indicate a slope of 3.4±0.9 upon exciting at 850 nm. This clearly indicates that the observed luminescence is due to a three-photon process (*cf.* Fig. 4).

The temporal profile of the MAIL spectrum was measured by means of streak camera detection. For all studied AuNPs, the time-resolved MAIL intensity resembles the response function of the streak camera, as obtained from Rayleigh scattering of AuNPs (FWHM=12 ps). This suggests that the MAIL is practically instantaneous. Indeed, the MAIL from AuNPs has been suggested as a very versatile instrumental response function for multi-photon excited luminescene lifetime experiments with ps time resolution, such as TCPSC, streak camera detection and fluorescence lifetime imaging [30]. A very short lifetime of the MAIL has also been reported by researchers [18, 20, 32].

The obtained MAIL efficiency ($E_{MAIL}(\lambda_{exc})$) at different excitation wavelengths (λ_{exc}) is exemplified in Fig. 5. The efficiency was calculated from the measured integrated MAIL intensity (I_{MAIL}) and the incident excitation power (W_A) according to:

$$E_{MAIL}(\lambda_{exc}) = I_{MAIL} W_A^{-2}. \tag{1}$$

In Eq. 1, the efficiency is normalized to an assumed two-photon excited process by dividing the luminescence signal by the square of the incident power. Here the used value of I_{MAIL} corresponds to the integrated intensity over wavelengths between 450 and 550 nm. For this range, the observed logarithmic power dependence is compatible with a two-photon process (Fig. 4). In order to examine different wavelength dependencies of the MAIL efficiency (for samples **I–IV**), the calculated efficiency curves were normalized to the sample´s maximum luminescence at λ_{exc}=630 nm, thereby removing the scaling with respect
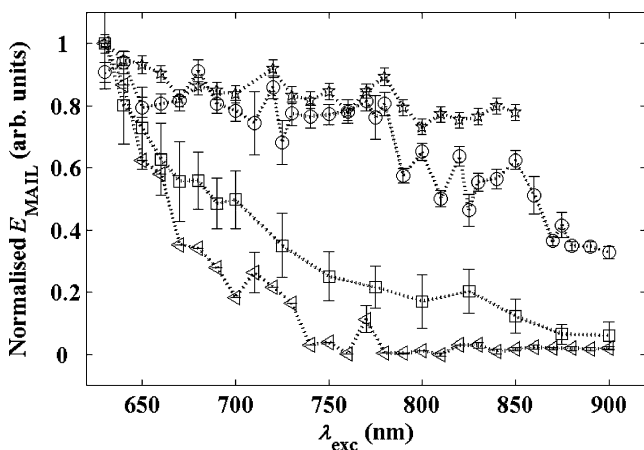

Fig. 5 Normalised MAIL efficiencies for samples **I** (squares), **2** (triangles), **III** (circles) and **IV** (stars). All the curves were normalised to unity at their corresponding maxima at 630 nm. Error bars correspond to two standard deviations of measured data points

to particle concentration and MAIL intensity (*cf.* Fig. 5). No particular physical mechanism motivates this normalization, which was only introduced for the sake of clarity. Depending on the samples compared, absolute MAIL intensities from the agglomerated structures were in average up to 1 order of magnitude higher than those from individually suspended coated or uncoated AuNPs for the excitation wavelength 630 nm.

As can be seen in Fig. 5, samples **I** and **II** with individually suspended AuNPs show a rapid decrease of E_{MAIL} with increasing λ_{exc}, resulting in a negligible emission at $\lambda_{exc} >$ 750 nm. On the other hand, the MAIL signal from the samples with agglomerates (**III** and **IV**) is significantly stronger over the whole range of excitation wavelengths. Furthermore, the MAIL intensity of sample **IV** remained rather constant over this spectral range. Thus, the MAIL efficiency is strongly dependent on the presence of NPs agglomerates. Moreover, the thickness of the silica coating did not affect MAIL intensity wavelength dependence. What is, however, the enhancement of the MAIL from agglomerated AuNPs relative to individual AuNPs at different excitation wavelengths? For illustrating this, a wavelength dependent enhancement factor $\eta(\lambda_{exc})$ is introduced as:

$$\eta(\lambda_{exc}) = E_{MAIL}^{aggl}(\lambda_{exc}) / E_{MAIL}^{indiv}(\lambda_{exc}) \qquad (2)$$

where $E_{MAIL}^{aggl}(\lambda_{exc})$ denotes the normalized MAIL efficiency from either sample **III** or **IV**, and $E_{MAIL}^{indiv}(\lambda_{exc})$ stands for the normalized MAIL efficiency from either sample **I** or **II**. Prior to calculating $\eta(\lambda_{exc})$, the experimental curves were approximated by polynomials of the 11th degree, which smoothes data and compensates for different choices of excitation wavelengths during different measurements. The resulting $\eta(\lambda_{exc})$ graphs are displayed in Fig. 6.

Taken together, a MAIL intensity enhancement by at least two orders of magnitude was calculated for samples **III** and **IV** relative to sample **II** at excitation wavelengths between 750 and 850 nm. A somewhat weaker enhancement was obtained for samples **III** and **IV** when compared with sample **I**.

Discussion

For the samples composed of individual nanoparticles (**I** and **II**), the MAIL efficiency increases with decreasing excitation wavelength and reaches it highest value at $\lambda_{exc} = 630$ nm (*cf.* Fig. 5), which is the shortest wavelength used in the present study. It is suggested that the near overlap between the laser excitation energy and the LSPR band of single AuNPs is the determining factor for the increased emission intensity at higher energies, *i.e.* at shorter excitation wavelengths. It is known that the spectral overlap increases the luminescence
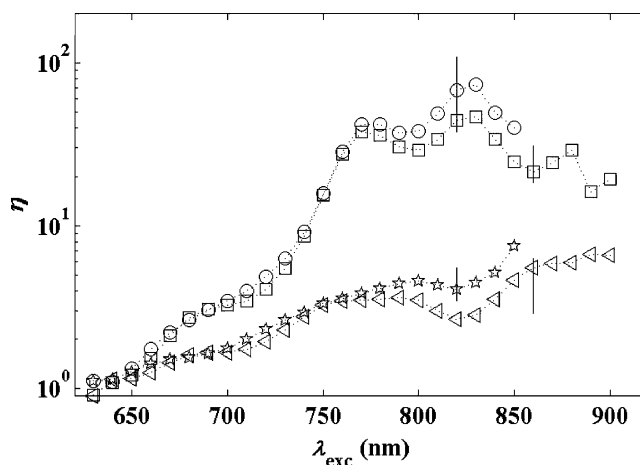

Fig. 6 The wavelength dependence of the enhancement factor $\eta(\lambda_{exc})$. The graphs were obtained as outlined in the text (Eq. 2). by dividing efficiencies from different samples in Fig. 5 as follows: $E_{MAIL}^{III}/E_{MAIL}^{I}$ (triangles), $E_{MAIL}^{III}/E_{MAIL}^{II}$ (squares), $E_{MAIL}^{IV}/E_{MAIL}^{I}$ (stars) and $E_{MAIL}^{IV}/E_{MAIL}^{II}$ (circles). Standard deviations are shown for selected data points

efficiency, particularly in the case of multi-photon excitation [9, 14, 19, 23]. In this case, the wider absorption band of sample **I**, relative to sample **II**, can explain the stronger MAIL from the former system (*cf.* Fig. 5).

The observed wavelength dependence of MAIL efficiency differ for the NPs agglomerates, as exemplified by samples **III** and **IV**. Similar to what was observed for samples **I** and **II**, the MAIL increases at shorter excitation wavelengths. However, there is no significant reduction in luminescence at longer excitation wavelengths, where the MAIL efficiency becomes almost wavelength independent (Fig. 5). Again it can be suggested that the nearly constant efficiency, as a function of wavelength, is due to the overlap of excitation energies with a modified LSPR of the agglomerated NP system [5–8, 23, 25, 26].

For nanoparticles, the position and width of the LSPR band depend on the NP size, interparticle distance, number of interacting particles, as well as their relative positions in space. The appearance of LSPR broad bands in the red and near IR part of the spectrum for agglomerated NPs was predicted theoretically and observed experimentally [5–9, 23–26]. For instance, the broad band centred at about 800 nm in the extinction spectrum of sample **III** (*cf.* Fig. 2) is attributed to an agglomerate surface plasmon excitation. Therefore, a coupling between this band and the radiation field could contribute to the observed enhancement of the MAIL from agglomerates. Similar conclusions have been drawn for SERS enhancement by similar systems of AuNP aggregates [25].

A similar dependence of the MAIL intensity on λ_{exc} and LSPR was observed from AuNPs embedded in a solid surface coated with SiO_2. In these studies, the luminescence

efficiency also showed a dependence on the excitation wavelength [23]{22}.

The wavelength dependence of MAIL efficiencies displayed in Fig. 5, and the calculated enhancement shown in Fig. 6 agree qualitatively with the calculations of the local electromagnetic field enhancement for various inter-particle separation between two AuNPs within a dimer [25]. For particles separated by 5 nm, calculations predict a drop in the field enhancement by several orders of magnitude in the range from 630 to 900 nm. This is a result of a weaker coupling between the individual AuNPs and the incident field. For separations less than 1 nm, field enhancement as a function of λ_{exc} exhibits broad peaks that corresponds to multipolar resonances in the extinction spectrum of the particles. An averaging with respect to a large number of agglomerated particles and interparticle distances might result in a wavelength independent local field enhancement in the red and near IR spectral regions. The local field enhancement of agglomerates is by several orders of magnitude stronger than that of individual AuNPs. This behaviour qualitatively agrees with the results presented in Fig. 6. The maximum obtained enhancement in the region 800–850 nm is likely correlated with the observed extinction band in sample **III** (*cf*. Fig. 2). Thus, the calculated local field enhancement [25] correlates with the experimental enhancement obtained in the present work.

Three photon absorption induced luminescence from AuNPs has been reported upon excitation by NIR radiation [20, 23]. The high-energetic part of the emission spectrum, *i.e.* for the luminescence of shorter wavelengths, can be explained by a three photon excitation (*cf*. Fig. 4). It has also been proposed by Mooradian [15] that the electron and hole distributions are thermally smeared out and that the photo-excited holes are scattered into a broad range of states resulting in luminescence at shorter wavelengths.

Metal NPs are known to be a source for various nonlinear optical processes. In addition to the luminescence reported in this article, other processes such as SHG, sum-frequency generation (SFG), third-harmonic generation (THG) and four-wave mixing (4WM) have been observed [33, 34]. These processes are also interesting and can find applications in bio-sensing and microscopy due to their directionality and large spectral shift from the fundamental beam(s). It has also been observed that NPs in contact can exhibit a very intense field enhancement where the localized field can give rise to a strong nonlinear response [32].

In our experiments, using the TOPAS as the excitation source, we have observed several nonlinear processes from AuNPs. For example, when the idler wavelength equals $2\lambda_{exc}$, the generated signal appeared at a wavelength that could correspond to several physical processes, such as degenerated 4WM, SHG (involving idler and fundamental beam), THG of the idler and higher diffraction orders of

Rayleigh scattering of the idler. These processes were also observed to be stronger from samples with the thickest silica coatings and agglomerates. Since the main subject of this paper is MAIL, care was taken to eliminate these processes by blocking the idler and signal beams generated by TOPAS, which propagate along the excitation beam used to generate MAIL. In many cases, these nonlinear processes can be much stronger than the MAIL, and could consequently lead to wrong interpretations of experimental results.

Conclusions

The MAIL intensity has been studied from naked individual, silica coated individual and agglomerated AuNPs suspended in water as the function of excitation wavelength. A strong MAIL efficiency from silica coated agglomerates was observed, which was weakly dependent on the excitation wavelength, while a rapid decrease in the MAIL intensity with the increasing excitation wavelength was observed from individual AuNPs. From the obtained data it was possible to determine the MAIL enhancement from agglomerates relative to individual NPs, as a function of the excitation wavelength. The maximum enhancement factor of at least two orders of magnitude was observed at the excitation wavelength between 800–850 nm. The results suggest that agglomerates exhibit plasmon excitations at wavelengths above 700 nm, which correlates with stronger MAIL. The magnitude and wavelength dependence of the enhancement agrees qualitatively with recent theoretical models available.

References

1. Ghosh SK, Tarasankar Pal T (2007) Interparticle coupling effect on the surface plasmon resonance of gold nanoparticles: from theory to applications. Chem Rev 107:4797–4862
2. Link S, El-Sayed MA (2003) Optical properties and ultrafast dynamics of metallic nanocrystals. Annu Rev Phys Chem 54:331–366
3. Sanders AW, Routenberg DA, Wiley BJ, Xia Y, Dufresne ER, Reed MA (2006) Observation of plasmon propagation, redirection, and fan-out in silver nanowires. Nano Lett 6:1822–1826
4. Sperling RA, Gil PR, Zhang F, Zanella M, Parak WJ (2008) Biological applications of gold nanoparticles. Chem Soc Rev 37:1896–1908
5. Felidj N, Aubard J, Levi G (1999) Discrete dipole approximation for ultraviolet–visible extinction spectra simulation of silver and gold colloids. J Chem Phys 111
6. Funston AM, Novo C, Davis TJ, Mulvaney P (2009) Plasmon coupling of gold nanorods at short distances and in different geometries. Nano Lett 9:1651–1658

7. Harris N, Arnold MD, Blaber MG, Ford JM (2009) Plasmonic resonances of closely coupled gold nanosphere chains. J Phys Chem C 113:2784–2791

8. Pecharroman C (2009) Influence of the close sphere interaction on the surface plasmon resonance absorption peak. Phys Chem Chem Phys 11:5922–5929

9. Addison CH, Konorov SO, Brolo AG, Blades MW, Turner RFB (2009) Tuning gold nanoparticle self-assembly for optimum coherent anti-stokes raman scattering and second harmonic generation response. J Phys Chem C 113:3586–3592

10. Chen CK, Heinz TF, Ricard D, Shen YR (1983) Surface-enhanced second-harmonic generation and Raman scattering. Phys Rev B 27:1965–1979

11. Fort E, Gresillon S (2008) Surface enhanced fluorescence. J Phys D: Appl Phys 41:13001–13032

12. Glass AM, Wokaun A, Heritage JP, Bergmann JG, Liao PF, Olson DH (1981) Enhanced two-photon fluorescence of molecules adsorbed on silver particle films. Phys Rev B 24:4606–4909

13. Chen CK, de Castro ARB, Shen YR (1981) Surface-enhanced second-harmonic generation. Phys Rev Lett 46:145–148

14. Boyd GT, Yu ZH, Shen YR (1986) Photoinduced luminescence from the noble metals and its enhancement on roughened surfaces. Phys Rev B 33:7923–7936

15. Mooradian A (1969) Photoluminescence of metals. Phys Rev Lett 22:185–187

16. Zhu G, Gavrilenko VI, Noginov MA (2007) Emission of Au nanoparticles with and without rhodamine 6G dye. J Chem Phys 127:104503–104508

17. Bouhelier A, Bachelot R, Lerondel G, Kostcheev S, Royer P, Wiederrecht GP (2005) Surface plasmon characteristics of tunable photoluminescence in single gold nanorods. Phys Rev Lett 95:267405–267409

18. Dulkeith E, Niedereichholz T, Klar TA, Feldmann J, von Plessen G, Gittins DI, Mayya KS, Caruso F (2004) Plasmon emission in photoexcited gold nanoparticles. Phys Rev B 70:205424–205425

19. Beversluis MR, Bouhelier A, Novotny L (2003) Continuum generation from single gold nanostructures through near-field mediated intraband transitions. Phys Rev B 115433-115436.

20. Farrer RA, Butterfield FL, Chen VW, Fourkas FT (2005) Highly efficient multi-photon-absorption-induced luminescence from gold nanoparticles. Nano Lett 5:1139–1142

21. Yeshchenko OA, Dmitruk IM, Alexeenko AA, Losytskyy MY, Kotko AV, Pinchuk AO (2009) Size-dependent surface-plasmon-enhanced photoluminescence from silver nanoparticles embedded in silica. Phys Rev B 79:235438–235442

22. Bouhelier A, Beversluis MR, Novotny L (2003) Characterization of nanoplasmonic structures by locally excited photoluminescence. Appl Phys Lett 83:5041–5049

23. Xiao S, Gong H, Su X, Han J, Han Y, Chen M, Wang Q (2007) Two- and three-photon luminescence of Au nanoparticles and resonant energy transfer from CdSe quantum dots. J Phys Chem C 111:10185–10189

24. Blatchford CG, Campbell JR, Creighton JA (1982) Plasma resonance—enhanced Raman scattering by adsorbates on gold colloids: the effects of aggregation. Surf Sci 120:435–455

25. McMahon JM, Henry A-I, Wustholz KL, Natan MJ, Freeman RG, Van Duyne RP, Schatz GC (2009) Gold nanoparticle dimer plasmonics: finite element method calculations of the electromagnetic enhancement to surface-enhanced Raman spectroscopy. Anal Bioanal Chem 394:1819–1825

26. Prodan E, Radloff C, Halas NJ, Nordlander P (2003) A hybridization model for the plasmon response of complex nanostructures. Science 302:419–420

27. Jana NR, Gearheart L, Murphy CJ (2001) Wet chemical synthesis of high aspect ratio cylindrical gold nanorods. J Phys Chem B 105:4065–4067

28. Mine E, Yamada A, Kobayashi Y, Konno M, Liz-Marzán M (2003) Direct coating of gold nanoparticles with silica by a seeded polymerization technique. J Colloid Interface Sci 264:385–390

29. Makarov NS, Drobizhev M, Rebane A (2008) Two-photon absorption standards in the 550-1600nm excitation wavelength range. Optics Express 16:4029

30. Ryderfors L, Mukhtar E, Johansson LB-Å (2005) Two-photon excited fluorescence depolarisation experiments: II. The proper response function for analysing TCSPC data. Chem Phys Lett 411:51–60

31. Wilcoxon JP, Martin JE, Provencio P (2001) Optical proproties of gold and silver nanoclusters investigated by liquid chromatography. J Chem Phys 115:998–1008

32. Varnavski OP, Mohamed MB, E-Sayed MA, Goodson T III (2003) Relative enhancement of ultrafast emission in gold nanorods. J Phys Chem B 107:3101–3104

33. Palomba S, Danckwerts M, Novotny L (2009) Non-linear plasmonics with gold nanoparticle antennas. J Opt A: Pure Appl Opt 11:114030–114035

34. Lippitz M, van Dijk MA, Orrit M (2005) Third-harmonic generation from single gold nanoparticles. Nano Lett 5:799–803